19th Brazilian Congress of Thermal Sciences and Engineering
November 06th-10th, 2022, Bento Gonçalves - RS - Brazil

ENC-2022-0680
A PRELIMINARY NUMERICAL STUDY OF A CONSTANT-PRESSURE SUPERCRITICAL FLUID-BASED THERMAL ENERGY STORAGE RESERVOIR DURING CHARGING

Victor DUTRA[1]
victor.dutra@lepten.ufsc.br

Thaís D. LUZ[1]
thais.luz@lepten.ufsc.br

Alexandre K. DA SILVA[1]
a.kupka@ufsc.br

[1]*LEPTEN Laboratory of Energy Conversion Engineering, Department of Mechanical Engineering, Federal University of Santa Catarina, Florianópolis, SC, Brasil.*

Abstract. *In solar thermal powered plants, the usage of thermal energy storage (TES) is arguably mandatory as it can mitigate the intermittency of solar radiation. Therefore, over the years, different materials were studied for TES applications, including supercritical fluids, which present high thermal capacitance and energy density when operating in conditions close to the critical point, justified by their intense thermophysical properties variation in these conditions. In this context, thermodynamic studies considering supercritical fluids operating at constant pressure show promising results, since the variation of isobaric specific heat is more intense than the isochoric version. Therefore, because of the inexistence of fully transient numerical studies dealing with the isobaric application of supercritical fluids for TES systems, this study develops a transient numerical study of a TES reservoir with a moving boundary under natural convection, such that the pressure of the reservoir, which is filled with supercritical carbon dioxide, a popular fluid for power cycles, is maintained at constant pressure. The TES charging process is promoted by a small heat source, which is allocated at the bottom of the reservoir. Four operational conditions were simulated, since four initial temperatures of the fluid domain were tested for a constant pressure operation of 16 MPa. The preliminary results show that the heat transfer coefficient increases when the pseudocritical temperature is found between the initial temperature of the fluid and the temperature of the heat source.*

Keywords: *thermal energy storage, supercritical carbon dioxide, transient study, natural convection*

1. INTRODUCTION

Historically, the increase for energy has been met by fossil fuels, which emit gases harmful to the atmosphere worsening the greenhouse effect. Thus, the energy transition from fossil fuels to renewable sources becomes imperative to the future of humanity (The Economist, 2021). However, renewable power generation still has several shortcomings; solar energy, for example, presents a natural intermittency caused by the day-night cycle and weather conditions. Concerning this problem, Thermal Energy Storage (TES) systems work as a bridge between energy generation and consumption times. Such devices store surplus energy to be used when solar radiation incidence is low, especially in Concentrated Solar Power (CSP) plants, enabling them to operate at any time (Ganapathi and Wirz, 2012). This technology is crucial to CSP proliferation worldwide, as discussed extensively in the literature (Gil, et al. 2010) (Tse et al., 2014) (Lakeh et al., 2013).

The desirable characteristics of a TES system are high efficiency, large energy density per unit of volume or mass, low cost, long-period energy storage capacity, elevated energy transfer power, among others (Ganapathi and Wirz, 2012). Many strategies are in development to better achieve these goals, such as the utilization of thermochemical, latent and sensible (Jegadheeswaran and Pohekar, 2009) TES, the addition of high conductivity materials (Motahar et al., 2014) (Ghossein et al., 2017), and different types of heat exchangers (Ma et al., 2017) (Liuet al., 2012), for example. Concerning these requirements, supercritical fluids are highly qualified candidates. The high non-linearities observed in

their thermophysical properties in near critical conditions provide large enhancements on the heat transfer rate and energy density, and the possibility of using organic fluids reduces the cost compared with current market options, like molten salt (Tse et al., 2014).

Much has been studied about heat transfer phenomena and energy storage capacity of supercritical fluids. Dubrovina and Skripov (1965) showed that despite the usually low thermal conductivity of organic fluids, there is an enhancement of their heat transfer coefficient in supercritical conditions, caused by the high non-linearities of the thermophysical properties. Rousselet et al., (2013) and Warrier et al., (2013) studied experimentally and computationally the heat transfer of supercritical carbon dioxide (s-CO_2) under natural convection, and showed that the convective heat transfer coefficient, h, peaked when the fluid is found in a condition of temperature and pressure close to one of its pseudocritical points, which is a thermophysical condition that maximizes the specific heat of the material for a given temperature or pressure. Hobold and da Silva (2017) explored this characteristic peak of h and analyzed the behavior of a heat exchanger using s-CO_2: they showed that, given an inlet temperature, there is an operating pressure that minimizes the outlet temperature, maximizing the overall heat transfer coefficient.

In this context, there are several works studying supercritical fluids for TES, which show that not only the heat transfer rate might be augmented, but also the stored energy within. Furst et al., (2014) studied numerically a supercritical TES (sTES) using R134-a and found that operating at supercritical conditions vastly improves costs and, mass and volumetric stored energy densities. This is especially true when the TES operates at constant pressure, because the non-linearities are much more pronounced than at constant volume. This difference becomes even more apparent the closer the thermodynamic condition is to the critical point, where the difference between the isobaric and isochoric heat capacities is amplified. This phenomenon has repercussions on the supercritical region, close to the pseudocritical points, as have shown Lappalainen et al., (2020) with supercritical water.

Nevertheless, the majority of works about the application of supercritical fluids on TES systems either focus on its vast potentials, with thermodynamic analysis, or miss the most promising but challenging regime, which is at constant pressure. This study aims on this literature gap, simulating the transient performance of a TES system using s-CO_2, since this fluid is a benchmark regarding the study of supercritical fluids according to Luz et al., (2021). This TES system will operate at constant pressure, and, to do so, the lid moves like a piston, changing its volume. The results indicate that the spatially average instantaneous heat transfer coefficient, $\bar{h}$ [W/(m^2·K)], the energy density per unit of mass, H_m [kJ/kg], and per unit of volume, H_V [kJ/m^3], each presents different optimization operating conditions as to maximize their values. This work also proposes a new magnitude to measure a TES performance, named charge inertia.

2. GEOMETRY AND MODEL

This model was developed and solved using COMSOL Multiphysics® version 5.3 (COMSOL AB). The simulated geometry is shown in Fig. 1. It is a vertical cylinder with equal height, L, and diameter, D_c, of 0.3 m. The walls are considered adiabatic, and the heat source is located at the center of the bottom wall with a circular geometry of diameter D_{HS} = 0.1 mm; this heat source size was chosen to maintain the simulation's stability, given the limited computational resources available. An initial temperature for the fluid domain is chosen, T_o [K], and this heat source has a prescribed temperature, T_w [K], that is set as 50 K above the initial fluid temperature, and the simulation stops when the spatially averaged instantaneous temperature of the fluid, $\overline{T}_f$ [K], increases 5 K. Given the axisymmetric symmetry, only a slice of the 2D domain was simulated. A transient study was developed, and the heat transfer mechanism to which the fluid is subjected is natural convection with laminar flow.

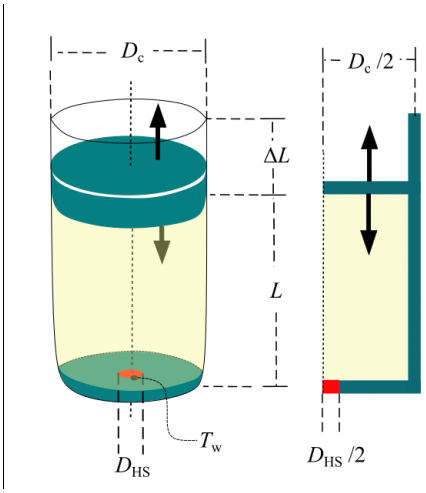

Figure 1. Geometry details.

To maintain the pressure p [MPa] constant, the lid moves as a piston, which is represented by the length variation ΔL on Fig. 1 and resulting in the volume variation. The lid movement is defined by a balance of forces on it, derived from the internal and external pressures – the external pressure is set as the desired constant pressure.

The governing equations of this problem are the conservation of mass, of momentum, and energy equations, as written on Eqs. (1), (2), and (3), respectively (Maliska, 2004). The working fluid is s-CO_2, whose properties are evaluated using CoolProp library (Bell et al., 2014).

$$\frac{\partial \rho}{\partial t} + \nabla \cdot (\rho \boldsymbol{u}) = 0 \tag{1}$$

$$\rho \frac{\partial \boldsymbol{u}}{\partial t} + \rho(\boldsymbol{u} \cdot \nabla)\boldsymbol{u} = \nabla \cdot \left[-\rho \boldsymbol{I} + \mu(\nabla \boldsymbol{u} + (\nabla \boldsymbol{u})^T) - \frac{2}{3}\mu(\nabla \cdot \boldsymbol{u})\boldsymbol{I}\right] + \rho \boldsymbol{g} \tag{2}$$

$$\rho C_p \left(\frac{\partial T}{\partial t} + \boldsymbol{u} \cdot \nabla T\right) + \nabla \cdot (-k \nabla T) = Q + Q_p \tag{3}$$

2.1 Thermodynamic states considered

The Rayleigh number is an important parameter to characterize the heat transfer in natural convection phenomena (Incropera and Deweitt, 1996) and it needs to be calculated for the storage media under the chosen operation conditions. Since the properties vary intensely in near critical conditions, for usage in the Rayleigh number calculation, the numerical values of the thermophysical properties of s-CO_2 were calculated as suggested by (Kato et al., 1968), by an integral average. Both the Rayleigh number equation and the integral average of a given property $\boldsymbol{\Phi}$ are presented on Eqs. (4) and (5) respectively.

$$Ra_{DHS} = \frac{g \bar{\beta} \Delta T {D_{HS}}^3}{\bar{\nu} \bar{\alpha}} \tag{4}$$

$$\bar{\phi} = \frac{1}{(T_w - \bar{T}_f)} \int_{T_w}^{\bar{T}_f} \phi\,(T) dT \tag{5}$$

In this work, four thermodynamic conditions were simulated, presented on Tab. 1: a pressure of 16 MPa was chosen, and four initial temperatures of the fluid domain were simulated for this pressure. Initially, three initial temperatures were selected with the intent to analyze the performance of the sTES around the pseudocritial temperature, T_{psc} [K], of the selected pressure, which is T_{psc} = 340.26 K. In one condition, here named $\mathfrak{C}_{anterior}$, the T_{psc} lies between T_o and T_w, and the $\bar{T}_f$ does not cross the T_{psc}; in another condition, $\mathfrak{C}_{crossing}$, the T_{psc} lies between T_o and T_w, and $\bar{T}_f$ crosses T_{psc}; in the third condition, $\mathfrak{C}_{posterior}$, T_o is larger than T_{psc}. Putting the chosen operation conditions in perspective, the critical point of s-CO_2 is 304 K and 7.38 MPa. However, given the high non-linearity of the thermophysical properties, the computational resources to simulate in conditions closer to this point were unavailable at the time. In this sense, the studied pressure still present variation of the thermophysical properties, but since they are not as intense it becomes easier to find numerical convergence of the results.

Table 1. Thermodynamic conditions simulated for the pressure p = 16MPa.

Symbol of thermodynamic condition	T_w **[K]**	T_o**[K]**	Ra_{DHS} **[-]**
$\mathfrak{C}_{Ra}$ **[K]**	371.7	321.7	2448.25
$\mathfrak{C}_{anterior}$ **[K]**	380.0	330.0	2448.78
$\mathfrak{C}_{crossing}$ **[K]**	388.0	338.0	2155.05
$\mathfrak{C}_{posterior}$ **[K]**	395.0	345.0	1753.45
T_{psc} **[K]**	-	340.26	2005.43

According to Warrier et al. (2013), the maximum heat transfer rate occurs when the T_{psc} is close to the arithmetic average between the values of T_w and the $\overline{T}_f$, this interval being defined as ΔT [K]; this trend also appeared when the results of the three initially simulated conditions were examined. Therefore, a fourth initial temperature was simulated for this pressure to study, in a scale of temperatures going from $\overline{T}_f$ to T_w, the effect of the position of T_{psc} in this ΔT. To isolate the effect of different Rayleigh numbers, this extra initial temperature was chosen to have the same initial Rayleigh as the condition $\mathfrak{C}_{anterior}$; but, in having a smaller T_o, the T_{psc} was closer to the center of the ΔT. Fig. 2 aids in the visualization of this concept, showing the initial Rayleigh on the y-axis, and the initial temperature on the x-axis, for the pressure of p = 16 MPa. The T_o for the four conditions simulated for this pressure are shown on the four plotted points; the simulated temperature range (5 K above T_o) of each condition is marked in the horizontal line segment of each point; and the pseudocritical temperature of this pressure is marked by the dotted red vertical line.

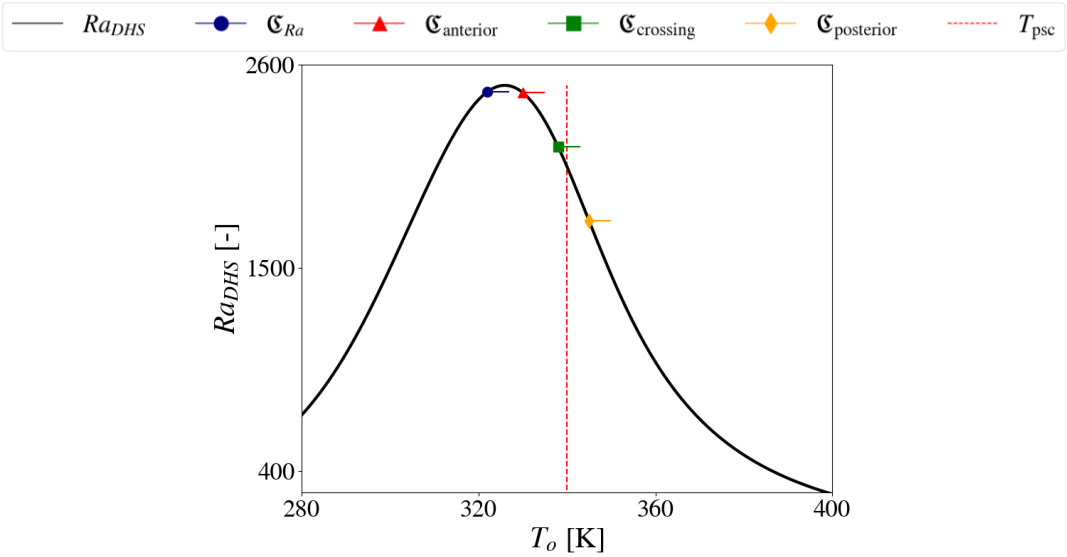

Figure 2. Initial Rayleigh based on initial temperatures, and the four simulated conditions for p = 16 MPa.

3. RESULTS AND DISCUSSION

3.1 Verification of the model

To ensure coherent results, convergence analysis of the spatial and temporal meshes were developed in the condition with the highest non-linearities: the one where $\overline{T}_f$ crosses T_{psc}. The mesh convergence was analyzed using s-CO_2, testing four spatial meshes, with 129648, 184404, 302635 and 438900 elements, and four temporal meshes, with $5x10^4$ s, $1x10^5$ s, $2x10^5$ s and $4x10^5$ s. Such large values for the time steps are required because of the very small diameter of the heat source, necessary for numerical stability of the simulation, which took sizable time to increase the temperature of the fluid. The analyses considered, also evaluated the lid displacement, x_t [mm], the energy stored, H [kJ], and the spatially averaged and instantaneous heat transfer coefficient on the wall, $\bar{h}$ [W/(m^2·K)], considering as an acceptable mesh one where the difference of the analyzed values is less than 1% to the next mesh, both for the spatial and temporal meshes. First, the temporal mesh convergence was studied, and the results can be seen in Fig. 3. It is clear from the graphics that all meshes had already converged. In this case, a time step of $2x10^5$ s was chosen to ensure the stability of the simulation in key moments. After this, the spatial mesh convergence was verified, and it is shown in Fig. 4, where the mesh with $3x10^5$ elements was selected since this is the one where the values of $\bar{h}$ converged with the following mesh.

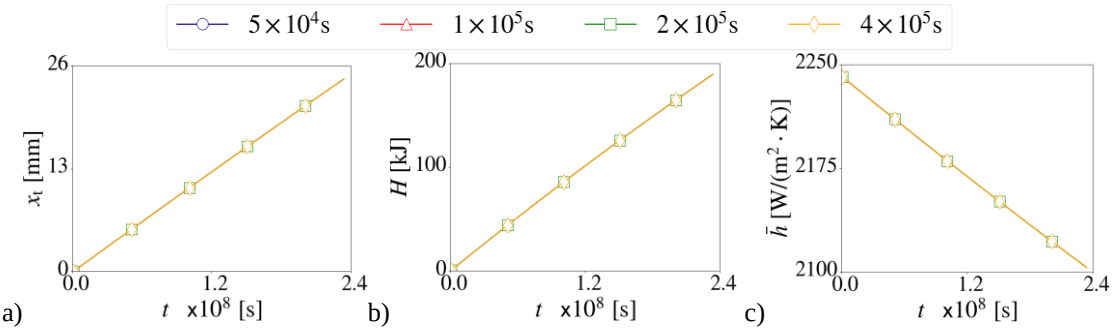

Figure 3. Temporal mesh verification: a) lid movement, x_t, b) stored energy H, and c) spatially averaged heat transfer coefficient $\bar{h}$, for the four timesteps tested: 5x10^{4}s, 1x10^5 s, 2x10^5 s and 4x10^5 s.

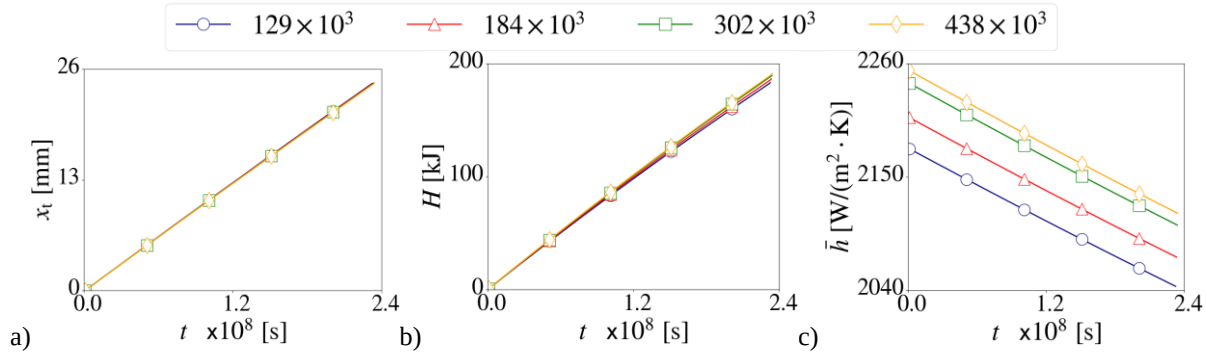

Figure 4. Spatial mesh verification: a) lid movement x_t, b) stored energy H, and c) spatially averaged heat transfer coefficient $\bar{h}$, for the four different meshes: 129648, 184404, 302635 and 438900 elements.

Since no other works were found on the litterature developing transient studies of the charging of a TES system operating at constant pressure and using supercritical fluids, there were no experimental or numerical studies that could be used for validation purposes. Therefore, this work attempts to verify the model by comparing the simulated results for the stored energy and the lid displacement with results calculated through the first law of thermodynamics (Nussenzveig, 2014) for different values of $\overline{T}_f$ and T_o = 338 K. The results of this analysis are shown in Fig. 5. The lid movement is very similar for both results, but the stored energy differs slightly. However, this difference is less than 10%, and is associated with the other phenomenons occuring in the simulation, such as the transient behavior of the simulations which is not accounted on thermodynamic analysis.

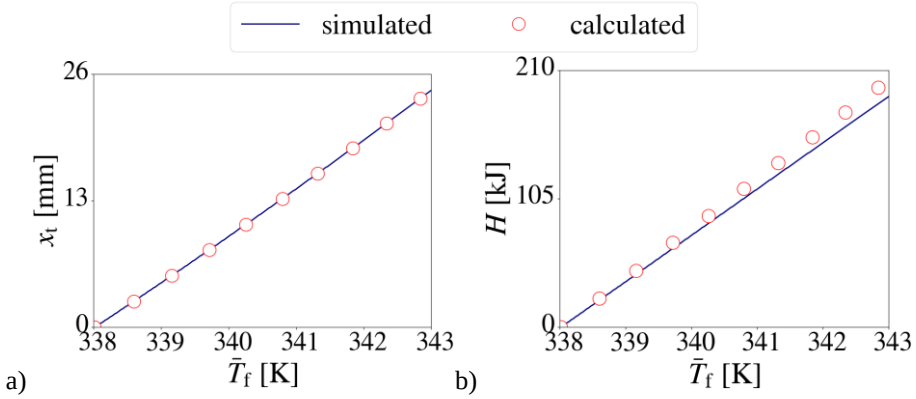

Figure 5. Thermodynamic verification, comparing the simulated values with the calculated ones. a) lid movement and b) stored energy.

3.2 Behavior of the thermophysical properties and their effect on the stored energy and convective heat transfer coefficient of s-CO_2 under natural convection

This section starts by showing the behavior of the density for the different temperatures studied for the pressure of 16 MPa, exploring its effect on the lid displacement. In this sense, Fig. 6a shows the spatially averaged instantaneous density, $\bar{\rho}$ [kg/m^3], of the fluid over the simulated time. The noticed density variations over the simulated time generate the movement of the lid, whose quantities are seen in Fig. 6b. As it can be observed, the lid movement is not only a

function of the absolute change in the density, but rather the percentual change, Δρ. Thus, it is the condition with the largest initial temperature, and the smallest density, that presents the largest lid movement.

Since the specific heat is an important parameter for heat transfer applications, Fig. 7 shows the (a) spatially averaged instantaneous isobaric specific heat for the different simulated conditions, $\bar{c}_p$ [J/(kg·K)], and (b) spatially averaged instantaneous isobaric specific heat per volume, $\bar{\rho}\cdot\bar{c}_p$ [MJ/(m^3·K)], both for each simulated temperature. On Fig. 7a it is possible to see that the $\bar{c}_p$ peaks on the pseudocritical temperature. Considering an analysis in terms of volume, the specific heat per unit of volume is the product of $\bar{c}_p$ and $\bar{\rho}$, and thus its behavior is the result of the tradeoff between them. This $\bar{\rho}\cdot\bar{c}_p$ can be visualized in Fig. 7b possibly peaking at the condition $\mathfrak{C}_{Ra}$; this reflects on the absolute stored energy, as seen in Fig. 8, where the (a) total stored energy stored H, (b) stored energy per unit of mass H_m, and (c) per unit of volume H_V, over the simulated time are plotted. It is noticeable that the volume variations are very similar between the simulated conditions since the lid displacement for all conditions simulated is in the order of millimeters as seen in Fig. 6b, which explains the similar behavior for the different conditions simulated found between the total energy (Fig. 8a) and the energy per unit of volume (Fig. 8c). Another curious result is found on Fig. 8a, which is that in the region close to the pseudocritical temperature, the smaller the initial temperature is, the higher the absolute and volumetric stored energy seems to be. This can be explained by the fact that $\bar{c}_p$ decreases with the initial temperature. However, lower initial temperatures require a higher amount of fluid in the tank to reach the same pressure. Then, it seems that this increase in the mass of fluid causes a higher impact than the decrease of $\bar{c}_p$ with the temperature, leading to the increase in the volumetric specific heat. Finally, one can observe that, in Fig. 8b, the inclinations of the H_m curves for different initial temperatures are very similar: this suggests that, as the mass of the fluid changes between the simulations due to the change in initial temperature, the average heat transfer rate of that simulation changes accordingly.

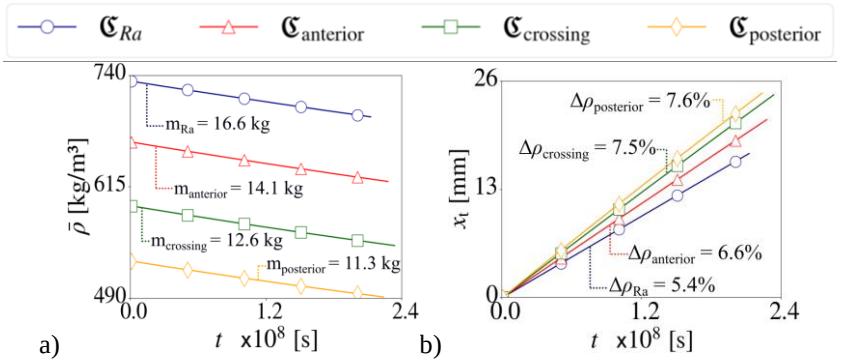

Figure 6. The simulated (a) density of s-CO_2 for each simulated condition, and (b) its variation effect on the lid displacement.

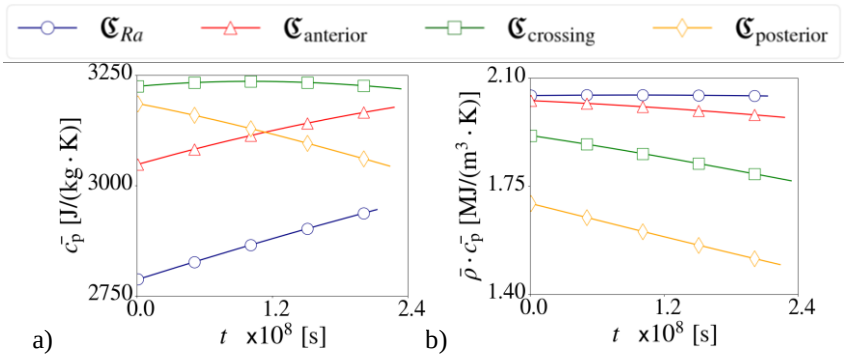

Figure 7. The isobaric specific heat for the simulated conditions (a) per unit of mass, and (b) per unit of volume.

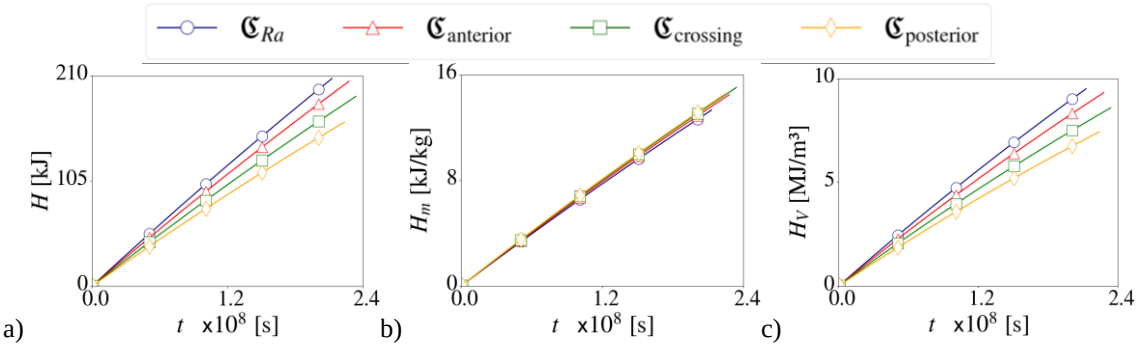

Figure 8. Stored energy over simulated time for each studied temperature and p = 16 MPa a) absolute stored energy, b) stored energy per mass and c) stored energy per volume

This can be verified when visualizing the behavior of the convective heat transfer coefficient, which is directly related to the heat transfer rate, Q [W], since $Q \sim h\Delta T$, and plotted in Fig. 9a for the different initial temperatures studied over the simulated time. It is noticeable that, as the T_o decreases, $\bar{h}$ grows. This result is in accordance with the conclusion reached by Warrier et al. (2013): even though the conditions $\mathfrak{C}_{Ra}$ and $\mathfrak{C}_{anterior}$ result in the same initial Rayleigh number, their heat transfer coefficients are different. Not only that, but the simulated temperature conditions do not seem to be approaching the maximum $\bar{h}$ so far, where this maximum value is expected to occur at a still smaller temperature. In accordance with Warrier et al. (2013), to maximize $\bar{h}$ it seems better to set the wall and the fluid temperatures to have the T_{psc} as a value found between T_w and $\overline{T}_f$. The peaks of heat transfer coefficient and isobaric specific heat per unit of volume occur when $\overline{T}_f$ is below the T_{psc}, suggesting that there is little advantage, from a heat transfer perspective, in crossing T_{psc} with $\overline{T}_f$ for a given pressure in a TES system.

Following this, it is evident from Fig 9a that the $\bar{h}$ is inversely proportional to T_o, reaching its smallest values among the different simulated conditions for the largest T_o and vice versa. The difference between the smallest and largest initial values found for $\bar{h}$ is approximately 30% of the smallest value. Differently, Fig. 9b shows the $\bar{h}$ divided by the $\bar{\rho}$ (previously shown in Fig 6a). It is noticeable that the $\bar{h}/\bar{\rho}$ ratio reaches its largest values with the largest T_o, diminishing with T_o, which is the contrary behavior found for $\bar{h}$. In this case, the difference between the smallest and largest initial values of $\bar{h}/\bar{\rho}$ is 5% of the smallest value. This indicates that the heat transfer coefficient and the density of the fluid are closely correlated. This makes sense when considering natural convection, since this phenomenon is governed by buoyancy. Besides, as it was discussed on Fig. 8b, the inclinations of H_m are very similar for the simulated temperatures, indicating that the stored energy per unit of mass grows at a similar rate for the different initial temperatures. This, in turn, supports the observation that the heat transfer rate changes at the same rate that the density does when T_o changes.

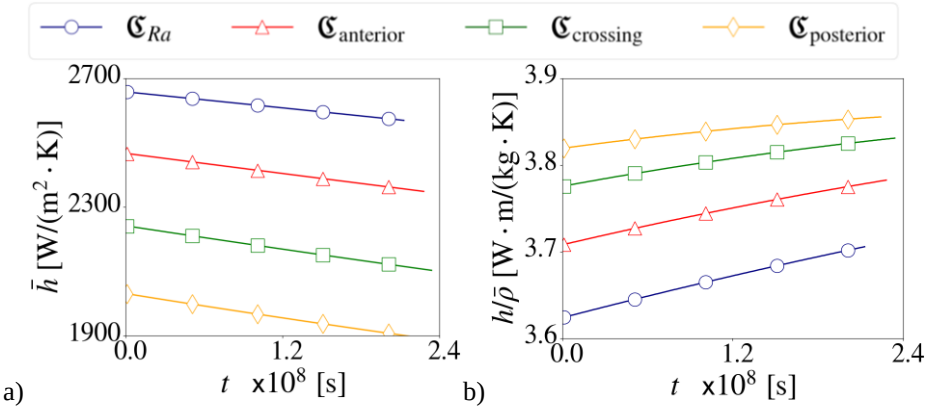

Figure 9. Heat transfer coefficient across time for each simulated condition. a) absolute heat transfer coefficient, and b) heat transfer coefficient divided by the density

3.3 The charge inertia as a performance parameter for TES medium

The literature about sTES vastly explores the stored energy density and the intensification of the heat transfer in near critical conditions. However, it lacks a manner to analyze both parameters combined in the transient performance of the TES system. Thus, this work proposes a new magnitude for evaluating the performance of TES systems, named charge inertia. This property signifies the stored energy (which can also be evaluated per unit of mass or volume)

divided by the heat transfer rate. Its absolute (I_{charge}), massic ($I_{charge,m}$) and volumetric ($I_{charge,V}$) values are presented in Eq. (6), (7) and (8), respectively, and have their transient behavior for each of the simulated temperatures for p = 16 MPa shown in Figs. 10a, 10b, and 10c respectively. Observe that the minimization of the inertia is desired to have the maximum heat transfer for a certain stored energy.

$$I_{charge} = \frac{\bar{c_p} \cdot m}{Q} \quad \left[\frac{s}{K}\right] \tag{6}$$

$$I_{charge,m} = \frac{\bar{c_p}}{\overline{Q}\overline{Q}} \quad \left[\frac{s}{kg \cdot K}\right] \tag{7}$$

$$I_{charge,V} = \frac{\bar{c_p} \cdot \bar{\rho}}{Q} \quad \left[\frac{s}{m^3 \cdot K}\right] \tag{8}$$

As the heat transfer rate, Q [W] has its value closely connected with the density, and consequently with the mass, the rates $Q/\bar{\rho}$ and Q/m remain approximately constant when T_o changes. On top of that, the volume variations are very similar between the simulated conditions, as previously discussed with Fig. 6b, which means the behaviors of $Q/\bar{\rho}$ and Q/m are also related, in a manner akin to the similarities found between H and H_V. Therefore, the I_{charge} and $I_{charge,V}$ behaviors are very similar, and it is mainly the $\bar{c_p}$ who defines the curve along the time for each T_o, as it is the single part in the equations that has a substantial change when T_o changes. The I_{charge} and $I_{charge,V}$ seem to reach a maximum close to the pseudocritical temperature, which is to be expected by the behavior of $\bar{c_p}$. The $I_{charge,m}$, on the other hand, has no reference to either mass or density in its equation, thus its unique performance: its value decreases with the initial temperature due to the dwindling of the $\bar{c_p}$ and rise of the heat transfer rate, showing no maximum between the simulated conditions.

All these results demonstrate that, although the massic stored energy peaks at T_{psc}, crossing this temperature with $\overline{T}_f$ is disadvantageous to the heat transfer rate, leading to the deterioration of the charge inertia. There seems to be no advantage either in using a T_o that surpasses the T_{psc}, as can be observed by the further deterioration of the $I_{charge,m}$ when T_o is still rising. These conclusions may have implications on the cost optimization for a TES system. Also, as discussed by Tse et al. (2013), due to the much smaller costs of organic fluids when compared with other similar solutions, the influence on the overall TES cost by optimizing the massic stored energy is limited. Thus, operating with T_{psc} between T_w and $\overline{T}_f$ offers the most advantages regarding heat transfer and stored energy; and approximating $\overline{T}_f$ to T_{psc} should be avoided, as it results in performance deterioration of the TES.

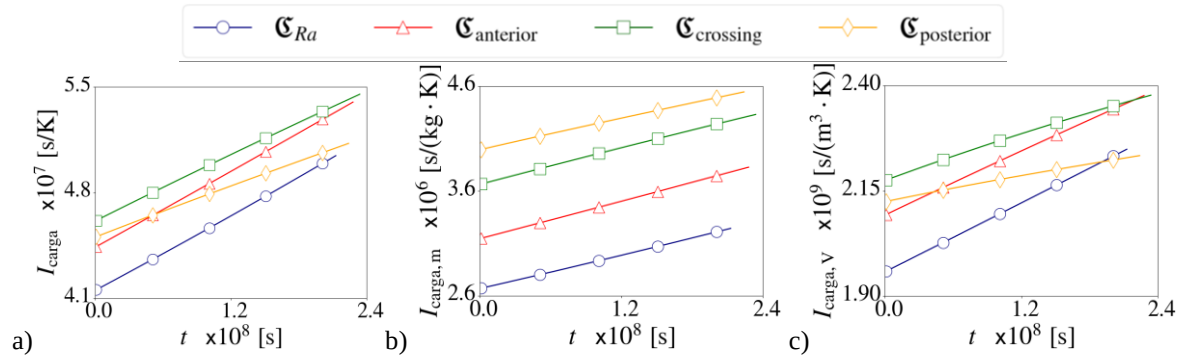

Figure 10. Charge inertia across time for each simulated condition. a) absolute charge inertia, b) charge inertia per mass and c) charge inertia per volume

4. CONCLUSIONS

This study analyzed the transient performance of supercritical carbon dioxide as TES medium under natural convection and constant pressure operation. For this chosen pressure p = 16 MPa, four different initial temperature were simulated to verify their influence in the performance both from heat transfer rate, energy stored per unit of mass and per unit of volume standpoints. Also, a new parameter called charge inertia was developed to aid in the performance evaluation of the system. In this sense, it seems advantageous, both to enhance the heat transfer rate as for the increase in the volumetric energy density to operate the system keeping the temperature of the fluid below the pseudocritical temperature for that operating pressure.

Further work is required to expand these simulated operation conditions to other pressures and temperatures to gain insight into the heat transfer behavior of supercritical fluids operating at constant pressure, and how this phenomenon interacts with the stored energy. This, in turn, will better elucidate how the charge inertia may contribute to the design and analysis of sTES systems. This study also helps to shed light on the unique conditions that affect the cost optimization calculus of a sTES system, requiring more work to explore this aspect, especially regarding the increasing importance of the volumetric heat capacity.

5. ACKNOWLEDGEMENTS

This study was financed in part by the Coordenação de Aperfeiçoamento de Pessoal de Nível Superior – Brasil (CAPES) – Finance Code 001. The support from Petrobras is also appreciated.

6. REFERENCES

Bell, I., Wronski, J., Quoilin, S., & Lemort, V. (2014). Pure and Pseudo-pure Fluid Thermophysical Property Evaluation and the Open-Source Thermophysical Property Library CoolProp. *Industrial & Engineering Chemistry Research*.

COMSOL AB. (n.d.). COMSOL Multiphysics v. 5.3. Stockholm, Sweden. Retrieved from www.comsol.com

Dubrovina, E., & Skripov, V. (1965). Convection and heat transfer near the critical point of carbon dioxide. *Journal of Applied Mechanics and Technical Physics*, 107-111.

Furst, B., Lavine, A., Lakeh, R., & Wirz, R. (2014). Isobaric, Isochoric and Supercritical Thermal Energy Storage in R134a. *ASME* (pp. 15-21). San Diego, California, USA: ASME.

Ganapathi, G. B., & Wirz, R. (2012). High Density Thermal Energy Storage With Supercritical Fluids. *ASME* (pp. 699-707). Houston, Texas: ASME. doi:10.1115/ES2012-91008

Ghossein, R., Hossain, M., & Khodadadi, J. (2017). Experimental determination of temperature-dependent thermal conductivity of solid eicosane-based silver nanostructure-enhanced phase change materials for thermal energy storage. *International Journal of Heat and Mass Transfer*, 697-711.

Gil, A., Medrano, M., Martorell, I., Lázaro, A., Dolado, P., Zalba, B., & Luisa, C. (2010). State of the art on high temperature thermal energy storage for power generation. Part 1—Concepts, materials and modellization. *Renewable and Sustainable Energy Reviews*, 31-55.

Hobold, G. M., & da Silva, A. K. (2017). A generalized multifluid optimal pressure for heat exchangers operating with supercritical fluid. *Numerical Heat Transfer, part A: Applications*.

Incropera, F., & Deweitt, D. (1996). *Fundamentals of heat and Mass Transfer.* New York: John Wiley & Sons, Inc.

Jegadheeswaran, S., & Pohekar, S. (2009). Performance enhancement in latent heat thermal storage system: A review. *Renewable and Sustainable Energy Reviews*, 2225-2244.

Kato, H., Nishiwaki, N., & Hirata, M. (1968). Studies on the Heat Transfer of Fluids at a Supercritical Pressure : 1st Report, A Proposition of Reference Values of Thermal Properties and Experiments with Supercritical Carbon-Dioxide. *JSME*, 654-663.

Lakeh, R., Lavine, A., Kavehpour, H. P., Ganapathi, G., & Wirz, R. (2013). Effect of Natural Convection on Thermal Energy Storage in Supercritical Fluids. *ASME.* Minneapolis, Minnesota: ASME.

Lappalainen, J., Baudouin, D., Hornung, U., Schuler, J., Melin, K., Bjelic, S., . . . Joronen, T. (2020). Sub- and Supercritical Water Liquefaction of Kraft Lignin and Black Liquor Derived Lignin. *Energies*.

Liu, M., Saman, W., & Bruno, F. (2012). Review on storage materials and thermal performance enhancement techniques for high temperature phase change thermal storage systems. *Renewable and Sustainable Energy Reviews*, 2118-2132.

Luz, T. D., Battisti, F., & da Silva, A. K. (2021). A numerical study of supercritical carbon dioxide as a medium for thermal energy storage applications under natural convection. *Numerical Heat Transfer, Part A: Applications* .

Ma, Z., Yang, W.-W., Yuan, F., Jin, B., & He, Y.-L. (2017). Investigation on the thermal performance of a high-temperature latent heat storage system. *Applied Thermal Engineering*, 579-592.

C.R. Maliska, Transferência de Calor e Mecânica dos Fluidos Computacional 2nd ed., LTC Editora, Sao Paulo, 2004.

Motahar, S., Nikkam, N., Alemrajabi, A., Khodabandeh, R., Toprak, M., & Muhammed, M. (2014). A novel phase change material containing mesoporous silica nanoparticles for thermal storage: A study on thermal conductivity and viscosity. *International Communications in Heat and Mass Transfer*, 114-120.

Nussenzveig, H. M. (2014). *Curso de Física Básica 2.* São Paulo: Blucher.

Rousselet, Y., Warrier, G., & Dhir, V. (2013). Natural Convection From Horizontal Cylinders at Near-Critical Pressures—Part I: Experimental Study. *Journal of Heat Transfer*, 135-145.

The Economist. (2021, 10 27). *The economics of the climate*. Retrieved from https://www.economist.com/special-report/2021/10/27/the-economics-of-the-climate

Tse, L., Ganapathi, G., Wirz, R., & Lavine, A. (2013). System Modeling for a Supercritical Thermal Energy Storage System. *ASME* (pp. 691-698). San Diego, California, USA: ASME.

Tse, L., Ganapathi, G., Wirz, R., & Lavine, A. (2014). Spatial and temporal modeling of sub- and supercritical thermal energy storage. *Solar Energy*, 402-410.

Warrier, G., Rousselet, Y., & Dhir, V. (2013). Natural Convection From Horizontal Cylinders at Near-Critical Pressures—Part II: Numerical Simulations. *Journal of Heat Transfer*.

7. RESPONSIBILITY NOTICE

The authors are the only responsible for the printed material included in this paper.